



Nonhomogenous transport current density and voltage distribution in isotropic high T_c superconductors

V. Bekeris^{a,*}, R. Schifini Gladchtein^a, M. Monteverde^a, P. Dmitruk^a, H. Ferrari^a, G. Polla^b, F. de la Cruz^c

^a *Facultad de Ciencias Exactas y Naturales, Universidad de Buenos Aires, Ciudad Universitaria, Buenos Aires 1428, Argentina*

^b *División de Física del Sólido, Departamento de Física Comisión Nacional de Energía Atómica, Buenos Aires 1429, Argentina*

^c *Centro Atómico Bariloche, 8400 San Carlos de Bariloche, Río Negro, Argentina*

Received 7 October 1996; revised 7 October 1997; accepted 9 December 1997

Abstract

Transport properties in patterned isotropic high T_c superconducting samples were investigated numerically and experimentally for boundary conditions imposing a nonhomogeneous current flow. Numerical simulations for the voltage distribution were based on a local nonlinear constitutive relation for the current density and the electric field, predicted by the vortex glass model extended to a nonhomogeneous current flow. In experiments the voltage drops at different sample locations were measured as a function of applied current, in a wide temperature range at low magnetic fields, and both the linear and the nonlinear regimes were examined. Our results support a local description, where long-range correlations in the millimeter scale are absent. © 1998 Elsevier Science B.V.

PACS: 74.25.Fy; 74.40.+k; 74.80.Bj

Keywords: Transport properties; Intergranular vortex phases

1. Introduction

Conventional transport properties in sintered, polycrystalline $\text{YBa}_2\text{Cu}_3\text{O}_{7-\delta}$ (YBCO) [1] and $\text{La}_{2-x}\text{Sr}_x\text{CuO}_{4-\delta}$ (LSCO) [2–4] high T_c superconductors are well described within the framework of the vortex glass model [5,6]. There is strong evi-

dence that the intergranular vortex system exhibits a second-order phase transition at the field dependent glass temperature, $T_g(H)$, where vortices freeze into a true zero resistance state, showing the scaling behavior predicted for a vortex glass: $E/(J|t|^{v(z-1)}) = F^+_{-}(J/|t|^{2v})$, where E and J are the electric field and the current density, $t = |T - T_g|/T_g$ and v and z are critical exponents [5,6].

At the phase transition temperature, the E – J characteristics show a power-law behavior. Above $T_g(H)$ an ohmic regime at low current density is observed, and below $T_g(H)$, the constitutive relation

* Corresponding author. Departamento de Física, Pabellón I, Ciudad Universitaria, Buenos Aires 1428, Argentina. Tel.: +54-01-782-1007; fax: +54-01-782-7647; e-mail: lbtuba@df.uba.ar.

for the electric field and the current density is given by the following expression

$$E \sim \exp\left(-\left(J_c/J\right)^\mu\right) \quad (1)$$

where μ is in the range 0–1, and J_c increases as temperature is reduced below the phase transition [5,6]. The length scale for intergranular currents is set by the grain size, d , but at low current densities, the activated vortex loop size L_j , becomes larger than d , and the sample appears homogeneous [1]. In the previous works [1–4] where conventional four-terminal transport experiments were performed, the boundary conditions (sample and current contacts geometry) determine a uniform macroscopic current flow, and the applied current dependence of the voltage drop, $V(I_a)$, can be compared to the $E(J)$ characteristics predicted by theory (see for example Fig. 3 in Ref. [1] and Fig. 1 in Ref. [3]).

However, future applications may be based on devices constructed with geometries imposing non-homogeneous transport current densities, not being clear what is the voltage distribution and its current dependence particularly in the highly nonlinear regimes. This possibility has led us to examine multi-terminal transport properties in a granular system, where it is possible to separate the influence of anisotropy from the nonhomogeneous current effects arising from the sample geometry. The length scale for the macroscopic current density variation is fixed by the boundary conditions, and we have examined geometries where this length is much larger than the grain size ($d \sim 10 \mu\text{m}$), so the homogeneous sample description remains valid.

This work is organized as follows: in Section 2 we present a numerical simulation for the current dependence of the bidimensional voltage distribution in the ohmic and the nonlinear regimes, for a sample with the same boundary conditions as one described in experiments. The hypothesis of a scalar apparent resistivity which depends on the total current density is supported by experimental results presented in Section 3. In Section 4 we report results of multi-terminal transport measurements in two samples of different geometries; we have measured the voltage drop at several sample locations as a function of applied current in a wide temperature range for low magnetic fields. Conclusions are presented in Section 5.

2. Calculations

Our numerical simulation was based on the equation of charge conservation: $\nabla \cdot \mathbf{J} = 0$ and a nonlinear constitutive relation for the local current density \mathbf{J} and the electric field \mathbf{E} , following Eq. (1) with $\mu = 1$. This relation is valid only in the vortex-glass phase. Since $\mathbf{J} = \sigma(\mathbf{E})$, $\sigma = \sigma(E)$ for this nonlinear relation, and $\mathbf{E} = -\nabla V$, the conservation equation expressed in terms of the electric potential V is $\nabla \cdot (\sigma \nabla V) = 0$, which in a 2D case is

$$\frac{\partial}{\partial x} \left(\sigma \frac{\partial V}{\partial x} \right) + \frac{\partial}{\partial y} \left(\sigma \frac{\partial V}{\partial y} \right) = 0. \quad (2)$$

To solve numerically this differential equation we apply the finite volume method [7], using a square grid, to a sample with the geometry shown in the inset of Fig. 1.

Note that since $\sigma = \sigma(E) = \sigma(-\nabla V)$, the discretization equation is nonlinear. We solved this system iterating over the complete grid (Gauss–Seidel point by point method) until convergence with a relative tolerance of 10^{-5} is reached. We imposed Neumann boundary conditions at the walls where there is no net current flux (that is, $\partial V / \partial n = 0$, where n is the normal direction to the wall) and Dirichlet boundary conditions ($V = \text{constant}$) at the current contacts, where there is a net normal current flux entering or leaving the sample. By setting the voltage drop between the current contacts, the cur-

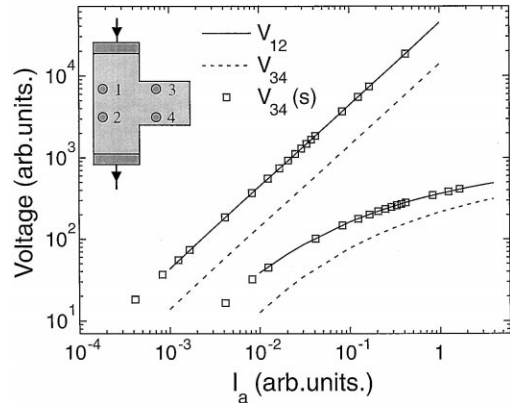


Fig. 1. Calculated V_{12} (full line) and V_{34} (dotted line) vs. applied current, I_a for the ohmic and the nonlinear regimes. Shown in symbols is $V_{34}(s)$ which stands for $g * V_{34}$ vs. I_a/f . The inset shows the sample and contacts geometry.

rent distributions were calculated and with this the different voltage drops between the voltage contacts. Total applied current, I_a , was calculated integrating the current density. The same procedure was followed for the linear case, where $\sigma = \sigma_0$.

Fig. 1 shows a log–log plot for V_{12} (full lines) and V_{34} (dotted lines) as a function of applied current, for both the linear and nonlinear regimes. Also shown, in symbols, is $V_{34}(s)$ which stands for $g * V_{34}$ vs. I_a/f , where f and g are two scaling factors that map the V_{34} vs. I_a curve onto the V_{12} vs. I_a curve in both regimes. For the linear response, it is clear that either a current scaling, (I_a/h) , or a voltage scaling $(h * V_{34})$ is enough to map V_{34} onto V_{12} , where $h = f * g$. Nevertheless, for the nonlinear response a unique set of values for f and g is needed in order to map one onto the other. In this particular case we have obtained $f = 2.4$ and $g = 1.3$. This is a general result for all the calculated voltage drops, and results from the scaling relation between the local current density and the applied current found in calculations. Therefore f and g depend only on the relative position of contacts (a change in temperature is represented by a change in σ_0 or in J_c , with no influence on f or g), and will be indicated as f_{34}^{12} and g_{34}^{12} in what follows. As $V_{ij}-I_a$ curves can also be mapped onto calculated $V-I_a$ curves for a slab, not shown, they can also be fitted to the expression predicted by the vortex glass model, where the fitted characteristic current density J_c , includes a site-dependent scaling factor.

3. Apparent resistivity

A polycrystalline $\text{La}_{1.8}\text{Sr}_{0.2}\text{CuO}_{4-d}$ sample, prepared as described elsewhere [8], was cut in the shape shown in the inset of Fig. 2 and ground to ~ 0.5 mm. The average grain size was $10 \mu\text{m}$. Two current and two voltage pairs of gold contacts were sputtered onto the surface of the sample over which silver baking paste was annealed at 650°C for 2 h to improve contact resistance, which resulted below 0.5Ω . Two Keithley 224 current sources were used to apply current independently in the x , (I_x), and y , (I_y), directions. Although the current density is not uniform around the sample corners, it is approximately uniform in the region between voltage contacts.

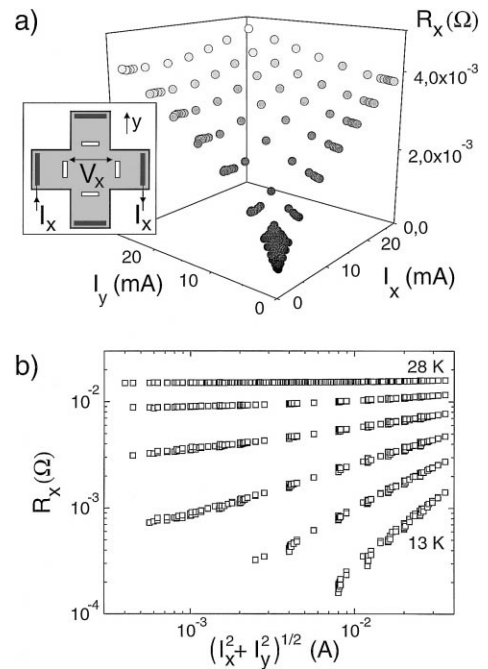


Fig. 2. (a) $R_x = V_x/I_x$ vs. I_x and I_y in the low temperature nonlinear regime where R_x depends on $(I_x^2 + I_y^2)^{1/2}$. The inset shows schematically the sample geometry; (b) V_x/I_x vs. $(I_x^2 + I_y^2)^{1/2}$ for $T = 13, 16, 19, 22, 25$ and 28 K and $H_a = 400$ Oe.

The voltage drops were measured using a digital scanner and a Keithley 181 nanovoltmeter with approximately 20-nV resolution. Magnetic DC field, H_a , provided by a superconducting solenoid, was applied perpendicular to the sample in the normal state, and the sample was field cooled to several temperatures.

V_x and V_y were measured as a function of increasing I_x for different I_y . Because of symmetry we refer only to the V_x results. I_y generated no voltage drop in the x direction (Hall effects are negligible [9]), and R_x was evaluated as V_x/I_x after proper current inversion to make negligible spurious thermal e.f.m. effects.

Fig. 2(a) shows $R_x(I_x, I_y)$ for $T = 19$ K and $H_a = 400$ Oe, and in Fig. 2(b) we plot R_x vs. $(I_x^2 + I_y^2)^{1/2}$ for $T = 13, 16, 19, 22, 25$ and 28 K and $H_a = 400$ Oe. It is clear that R_x is a function of the absolute value of the total applied current. Similar results were obtained for $H_a = 0$ and 100 Oe, supporting a total current density dependence of the resistivity.

4. Multiterminal I – V characteristics

For the experimental study of the voltage distribution, two polycrystalline $\text{La}_{1.8}\text{Sr}_{0.2}\text{CuO}_{4-d}$ samples [8] from different batches were cut in the shapes shown in Fig. 3 and ground to ~ 0.5 mm (sample A) and ~ 0.7 mm (sample B). Two low-resistance wide-current contacts and six 0.2-mm-diameter voltage contacts, made following the procedure described in Section 3, are shown schematically in the figure for sample A. Sample B was provided with two pairs of voltage contacts.

In the ohmic regime the superconducting transition voltage drop was measured across several contact pairs for $H_a = 0$ and $I_a = 500 \mu\text{A}$. Fig. 4 shows in full lines V_{12} , V_{34} and V_{56} as a function of temperature for sample A. Contacts 12 were arbitrarily chosen as reference, and shown in symbols is $h_{ij}^{12} * V_{ij}$ vs. T (ij standing for 34 and 56), where $h_{34}^{12} = 2.4$ and $h_{56}^{12} = 10.7$ are the voltage scaling constants, indicating that the average current density, $\langle J_{ij} \rangle$ is lower than $\langle J_{12} \rangle$. As expected for a linear regime, h_{ij}^{12} is temperature independent up to 300 K (not shown in the figure). Similar results were obtained for the resistive transition of sample B, with $h_{34}^{12} = 5.8$.

We present next the multiterminal I – V characteristics for sample A at $H_a = 400$ Oe. We show in Fig. 5 the log–log plot of: (a) V_{12} vs. I_a ; (b) V_{34} vs. I_a and (c) V_{56} vs. I_a for temperatures between 14 and 27 K. For every temperature, voltage is first detected between contact pair 12, and current has to be further increased so that dissipation across the next pair of voltage contacts exceeds voltage resolution.

The collection of curves at each location was mapped onto the collection of V_{12} vs. I_a curves, as

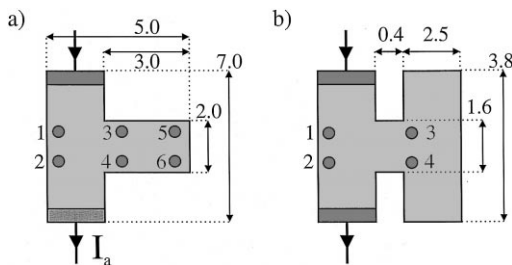


Fig. 3. Layout of the geometry, current and voltage contacts for (a) sample A; (b) sample B. Lengths are given in mm.

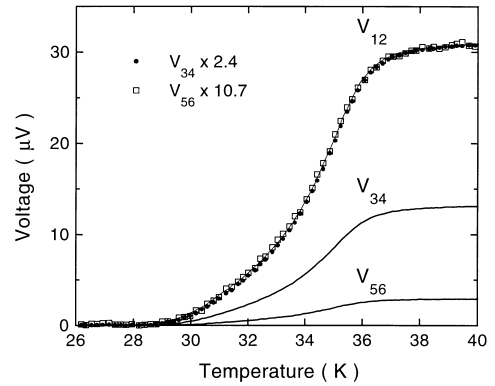


Fig. 4. V_{ij} vs. temperature for $I_a = 500 \mu\text{A}$ and $H_a = 0$ for sample A, where $ij = 12, 34, 56$ (solid). Also shown is $h_{34}^{12} * V_{34}$ (\bullet), and $h_{56}^{12} * V_{56}$ (\square), where $h_{34}^{12} = 2.4$ and $h_{56}^{12} = 10.7$.

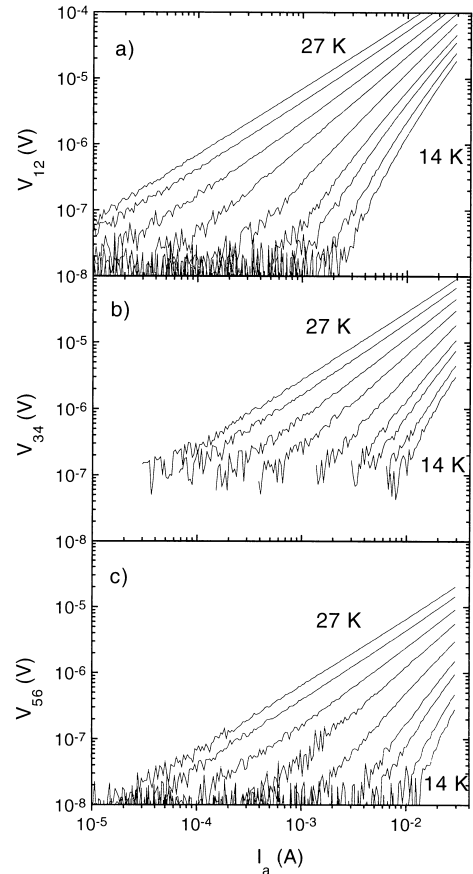


Fig. 5. (a) V_{12} vs. I_a ; (b) V_{34} vs. I_a and (c) V_{56} vs. I_a . In all cases, $T = 14, 15, 16, 17, 19, 21, 23, 25$ and 27 K, with $H_a = 400$ Oe for sample A.

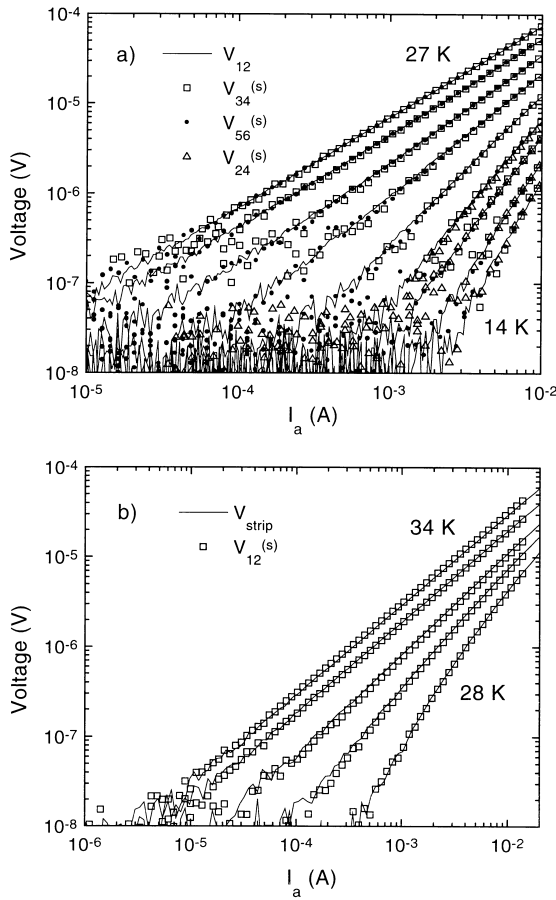


Fig. 6. (a) V_{12} vs. I_a (solid line) and $V_{ij}(s)$, which stands for $g_{ij}^{12} * V_{ij}$ vs. I_a / f_{ij}^{12} (symbols), at $T = 14, 15, 16, 17, 19, 21, 23, 25$ and 27 K, with $H_a = 400$ Oe for sample A. (b) V vs. I_a (solid line) for a strip of the same batch as sample B. Also shown is $g * V_{12}$ vs. I_a / f (in symbols) for sample B, $H_a = 0$.

shown in Fig. 6(a). Table 1 shows the site dependent scaling factors. The product $f_{ij}^{12} * g_{ij}^{12} = h_{ij}^{12}$, where h_{ij}^{12} is the ohmic scaling factor (see Fig. 4). Similar results were obtained for sample B at 20, 40, 60 and

Table 1
Geometrical scaling constants f_{ij}^{12} and g_{ij}^{12} for different contact pairs ij for sample A

Scaling factor	Contacts				
	34	56	24	46	26
f	2	3.5	0.7	1.5	0.9
g	1.3	3.1	4.1	3.4	2.2

Applied current must be divided by f_{ij}^{12} and voltage must be multiplied by g_{ij}^{12} to map each curve onto $V_{12}(I_a)$.

Table 2

Geometrical scaling constants f_{ij}^{12} and g_{ij}^{12} for different contact pairs ij for sample B

Scaling factor	Contacts		
	34	13	24
f	4.2	0.5	1.0
g	1.4	5.0	2.2

Applied current must be divided by f_{ij}^{12} and voltage must be multiplied by g_{ij}^{12} to map each curve onto $V_{12}(I_a)$.

80 Oe, and the field independent scaling factors are presented in Table 2.

In Fig. 6(b) we show $V-I_a$ characteristics for a strip $7 \times 2 \times 0.7$ mm³ of the same batch as sample B (full lines) at $H_a = 0$ and different temperatures, which can be described within the vortex-glass model [2–4]. Also shown (symbols) is $0.88 * V_{12}$ vs. $I_a / 1.7$ for sample B. If we fit the data V vs. I_a (slab) and V_{12} vs. I_a (sample B) to the expression $V = V_0 \exp(-(I_c / I_a)^\mu)$, for $T = 28$ K, we obtain for the slab a characteristic current I_c (slab) approximately equal to $(1/2) * I_c$ (Sample B). The mapping procedure provides a comparative description that is useful to avoid fitting every measured curve.

It is well established [10] that the low current-density regime at $T > T_g(H)$, crosses over to a nonlinear regime for $J > J_{cr}$, but it was not observed in the present work due to our voltage resolution. Nevertheless, the result $f_{ij}^{12} * g_{ij}^{12} = h_{ij}^{12}$ is an indication that the scaling procedure will map the complete curves.

5. Conclusions

We have studied the transport properties in isotropic LSCO high- T_c superconducting samples which were patterned to force a nonhomogeneous transport current flow, and were provided with several voltage contact pairs, ij , to measure the applied current dependence of the voltage distribution. We have found that the $V_{ij}-I_a$ characteristics map onto conventional homogeneous current flow $V-I_a$ characteristics, and therefore follow the predictions of the vortex glass model, with scaled relevant parameters. Numerical simulations based on a constitutive relation for the current density and the electric field predicted for the vortex glass phase and for the ohmic regime, also exhibit mapping properties arising from the proportionality between applied current

and local current density found in calculations. Our present results support a local electrodynamical description and the absence of long-range correlations in the intergranular vortex motion in the mm length scale. Future measurements in patterned films, where the voltage contact distances may be reduced below the millimeter scale will be performed.

Acknowledgements

We thank G. Gnani and A. López Dávalos for fruitful discussions. We acknowledge E. Rodríguez for careful reading of the manuscript. This work was partially supported by CONICET PID 303320088 and UBA EX018 grants.

References

- [1] T.K. Worthington, E. Olson, C.S. Nichols, T.M. Shaw, D.R. Clarke, *Phys. Rev. B* 43 (1991) 10538.
- [2] R. Decca, PhD Thesis, Instituto Balseiro, Universidad Nacional de Cuyo, Argentina, 1994.
- [3] R. Decca, *Physica C* 235–240 (1994) 1639.
- [4] L. Urba, C. Acha, V. Bekeris, *Physica C* 279 (1997) 95.
- [5] M.P.A. Fisher, *Phys. Rev. Lett.* 62 (1989) 1415.
- [6] D.S. Fisher, M.P.A. Fisher, D.A. Huse, *Phys. Rev. B* 43 (1991) 130.
- [7] S.V. Patankar, *Numerical Heat Transfer and Fluid Flow*, Hemisphere Publishing, Mc Graw-Hill, New York, 1981.
- [8] R. Crubellati, P. Smichowski, D. Batistoni, G. Polla, E. Manghi, *Solid State Commun.* 75 (1990) 101.
- [9] M. Petracic, A. Hamzic, B. Leontic, L. Forro, *Int. J. Mod. Phys. B* 1 (34) (1987) 1067.
- [10] G. Blatter, M.V. Feigelman, V.B. Geshkenbein, A.I. Larkin, M.V. Vinokur, *Rev. Mod. Phys.* 66 (1994) 1125.